Structural Determination of a Transient Isomer of CH_2I_2 by Picosecond X-Ray Diffraction

Jan Davidsson,[1,*,†] Jens Poulsen,[2,3] Marco Cammarata,[4] Panayiotis Georgiou,[1] Remco Wouts,[5] Gergely Katona,[2] Frida Jacobson,[2] Anton Plech,[6,7] Michael Wulff,[7] Gunnar Nyman,[3] and Richard Neutze[2,*,‡]

[1]*Department of Physical Chemistry, Uppsala University, Box 579, 75123 Uppsala, Sweden*
[2]*Department of Chemistry and Bioscience, Chalmers University of Technology, Box 462, 40530 Gothenburg, Sweden*
[3]*Department of Chemistry, Göteborg Univeristy, Box SE 412 96 Gothenburg, Sweden*
[4]*Department of Physical and Astronomical Sciences, National Institute for the Physics of Matter, via Archirafi 36, 90123, Palermo, Italy*
[5]*Department of Cell and Molecular Biology, Uppsala University, BMC, Box 596, 75 124 Uppsala, Sweden*
[6]*Fachbereich Physik, Universitaet Konstanz, D-78457 Konstanz, Germany*
[7]*European Synchrotron Radiation Facility, Grenoble Cedex 38043, BP 220, France*

(Received 11 November 2004; published 24 June 2005)

Ultrafast time-resolved spectroscopic studies of complex chemical reactions in solution are frequently hindered by difficulties in recovering accurate structural models for transient photochemical species. Time-resolved x-ray and electron diffraction have recently emerged as techniques for probing the structural dynamics of short lived photointermediates. Here we determine the structure of a transient isomer of photoexcited CH_2I_2 in solution and observe the downstream reactions of the initial photoproducts. Our results illustrate how geminate recombination proceeds *via* the formation of a transient covalent bond onto the iodine atom remaining with the parent molecule. Further intramolecular rearrangements are thus required for the CH_2I-I isomer to return to CH_2I_2. The generation of I_3^- from those iodine radicals escaping the solvent cage is also followed with time.

DOI: 10.1103/PhysRevLett.94.245503 PACS numbers: 61.10.Eq, 78.47.+p, 82.53.Eb

Almost all chemical reactions in biology as well as most industrial applications occur in the liquid phase. Since the advent of time resolved experimental techniques, the study of chemical reaction dynamics in liquids has generated tremendous experimental and theoretical interest. A major limitation of time-resolved spectroscopy is that structural changes specific to photochemical species cannot be determined directly but must be inferred from theoretical models of the relevant energy surfaces. In this context, the recent demonstration of ultrafast electron and x-ray scattering technologies in which structural changes were observed for photochemical species in vacuum [1–4] and in liquids [5,6] offers much promise.

Proof-of-principle liquid phase time-resolved x-ray diffraction experiments with 150 ps temporal resolution have been reported for iodine (I_2) in solution [5,6]. In those studies both reactants and products had an almost identical chemical structure with a perturbation in the iodine-iodine bond length for the excited state molecule being observed. A more complex photochemical problem is posed by the study of CH_2I_2 in solution, which is a precurser for the synthesis of many commercial carbohydrate halide derivatives. For example, the high yield cyclopropanation of a variety of olefins in the presence of diiodomethane irradiated by UV light has previously been reported [7–9]. Dihalomethanes are also of interest in atmospheric chemistry, for reactions in both the gas and the condensed phase, since they may be an important natural source of organohalide compounds emitted into the atmosphere [10–13].

Figure 1 presents a schematic of the photoreaction of CH_2I_2 [14]. Following excitation onto the antibonding C-I(σ^*) surface, an iodine atom is repelled and its covalent bond to the central carbon is broken. Consequently, the iodine radical ($I\cdot$) may either break out of the cage formed by the surrounding solvent molecules (path C, Fig. 1), or it may recombine geminately with the parent molecule $CH_2I\cdot$ (path A or B, Fig. 1). Following the initial time-resolved spectroscopic studies of this photochemical system [15–17], ambiguity emerged as to the nature of an early yet long-lived spectroscopic species and a number of conflicting models purporting to explain the available transient absorption spectroscopic data were proposed. Schwartz *et al.* [16] suggested that all transient spectroscopic features could most simply be interpreted as a $CH_2I\cdot$

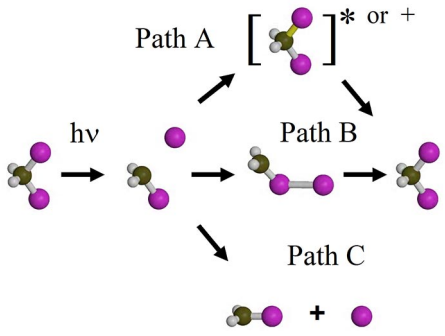

FIG. 1 (color online). Proposed reaction pathways following the photodissociation of CH_2I_2 in solution. Path A, $I\cdot$ recombines geminately onto the carbon atom of the parent $CH_2I\cdot$ radical, creating either an excited (*) or ionic ($^+$) state; Path B, $I\cdot$ recombines geminately onto the iodine atom of the parent $CH_2I\cdot$ radical, creating CH_2I-I; Path C, $I\cdot$ escapes the solvent cage.

radical that undergoes geminate recombination with I· onto a hot parent molecule, $CH_2I_2^*$, followed by slow thermal cooling (path A, Fig. 1). Conversely, Saitow *et al.* [18] ascribed the spectral feature to the formation of an ionic intermediate, $CH_2I_2^+$ (path A, Fig. 1). These interpretations were challenged by Tarnovsky *et al.* [19,20], who argued for the existence of a CH_2I-I isomer formed by geminate recombination following dissociation of the initially excited CH_2I_2 (path B, Fig. 1). More recent investigations using transient resonance Raman spectroscopy [20–23] as well as theoretical calculations [14,24–27] support this interpretation.

Direct evidence for the existence of the CH_2I-I isomer is provided by determining the x-ray structure of the intermediate using time-resolved x-ray diffraction [5,6]. In this work, synchrotron generated x-ray pulses of 150 ps duration were scattered from a liquid sample of 50 mMol CH_2I_2 dissolved in methanol. Data were collected at beam line IDO9B of the European Synchrotron Radiation Facility and the experimental geometry was as previously described [6]. Two hundred milliliters of 50 mMol CH_2I_2 (97% pure, purchased from FLUKA) in methanol (analytical grade purchased from FLUKA) was cycled through a flow cell narrowing to a 300 μm diameter quartz capillary at the sample position. 25 μJ, 100 fs laser pulses centered at 267 nm (third harmonic of the Ti:sapphire laser system) were used for sample photolysis. Following an electronically set time delay $\Delta t(\pm 3$ ps), polychromatic x-ray pulses (approximately 10^9 16.22 keV photons per 150 ps pulse, $\Delta E/E \sim 3\%$, 896 Hz repetition rate) were scattered from the sample onto a 133 mm MAR CCD x-ray camera located 45 mm from the sample position. After a 15 s integration prior to reading the camera, each image was integrated in concentric rings using Fit2D [28]. Data were typically averaged over ten images after being checked for parasitic signals, and were normalized according to the total counts from 6.3 $\text{Å}^{-1} < q < 7.6$ Å^{-1}, which is insensitive to structural changes [6]. The resulting radial intensity $S(q, \Delta t)$ was expressed as a function of the magnitude of momentum change of the deflected beam $q = (4\pi/\lambda) \times \sin\theta$, 2θ is the angle of deflection of the x-ray beam and λ its wavelength) and the time delay between photolysis and x-ray scattering (Δt). Data were taken for seven time delays: $\Delta t = -250$ ps; $\Delta t = 250$ ps; $\Delta t = 1$ ns; $\Delta t = 10$ ns; $\Delta t = 50$ ns, $\Delta t = 100$ ns, and $\Delta t = 1$ μs, with an additional time point $\Delta t = -3$ ns being recorded between every other image. These time points, i.e., laser arriving after the x-rays had scattered, were used as an updated reference against which all difference data were determined, thereby avoiding systematic errors or drifts within the data.

In Figs. 2(a) and 2(b) the experimental changes in x-ray diffraction intensities, $\Delta S(q, \Delta t)$, (photoexcited minus nonexcited) are represented. Data at -250 ps serve as a control for which a null signal is recovered. Multiplying $\Delta S(q, \Delta t)$ by q (to enhance the contribution of the higher q values) and $\exp(-\beta^2 q^2)$ (to dampen higher-frequency oscillations, $\beta = 0.15$ Å) and taking the Fourier transform from 2.35 $\text{Å}^{-1} < q < 7.7$ Å^{-1} (which avoids complications due to solvent expansion for $\Delta t \geq 50$ ps) provides an intuitive representation of the change in radial electron density $\Delta\rho(r)$ [6,29] seen by an "average excited atom" [Fig. 2(c)]. Since iodine strongly scatters x rays, this representation highlights the structural changes specific to iodine-iodine interatomic distances. From Fig. 2(c) it is evident that for $\Delta t \leq 10$ ns there is a strong depletion of electron density at $r = 3.7$ Å, with a corresponding increase at 2.9 Å. These features are the fingerprint of a shortened iodine-iodine separation of the photoisomer relative to the parent molecule.

Molecular dynamics simulations were undertaken to sample the geometry of the solvent packing around the respective photochemical species. Simulations were performed using MOSCITO [30] for CH_2I_2, CH_2I-I, $CH_2I\cdot$, $I\cdot$, and I^{3-} in methanol, as well as pure methanol. Snapshots from these simulations are illustrated in Fig. 3, with the initial molecule CH_2I_2 in methanol shown in Fig. 3(a); the photoisomer CH_2I-I in methanol shown in Fig. 3(b); and the $CH_2I\cdot + I\cdot$ species resulting from cage breakout shown in Fig. 3(c). Each simulation was performed for 6 ns in duration using a time step of 1 fs, and the temperature was set to both 300 and 310 K, with 215 solvent molecules +1 solute molecule in each simulation. To track the x-ray diffraction signal from thermal expansion, simulations were performed using six box volumes: $V = V_0$; $V_0 + 0.2\alpha\Delta T$; $\ldots V_0 + \alpha\Delta T$, where $V_0 = 216/\rho_0$, ρ_0 is the density of methanol = 0.7914 g · ml^{-1}, and α is the thermal expansion coefficient of methanol = 0.00149 K^{-1}. During these simulations, bond lengths and angles for CH_2I_2 and CH_2I-I were taken from Ref. [14].

X-ray scattering intensities $[S(q, \Delta t)]_{\text{theory}}$ were calculated using standard diffuse-x-ray scattering formulas [31] and explicitly incorporated scattering changes due to (i) structural changes within the photochemical species $[\Delta S^{\text{isomer}}(q)]$, (ii) scattering changes due to perturbations to the solvent packing around the photochemical species $[\Delta S^{\text{isomer-solvent}}(q)]$, and (iii) scattering changes due to structural changes in the solvent alone $[\Delta S^{\text{solvent}}(q)]$. The $\Delta S^{\text{isomer-solvent}}(q)$ term was of equal magnitude to $\Delta S^{\text{isomer}}(q)$ for simulations of $I\cdot$, CH_2I, and I^{3-} in the range 0.3 $\text{Å}^{-1} < q < 1.2$ Å^{-1}, but was less significant for CH_2I-I for which the solvent packing was less perturbed. $\Delta S^{\text{solvent}}(q)$ arises from the influence of heating and subsequent thermal expansion [32] and dominates the x-ray scattering from 0.3 $\text{Å}^{-1} < q < 2.35$ Å^{-1} for $\Delta t \geq 50$ ps. Heating occurs due to energy transfer from the photoexcited solute molecules to the solvent molecules, and thus the thermal expansion after 100 ns provides a measure of the total heat input into the system.

An optimal fit to all experimental data was determined by calculating $[\Delta S(q, \Delta t)]_{\text{theory}}$ (red lines, Fig. 2) upon the

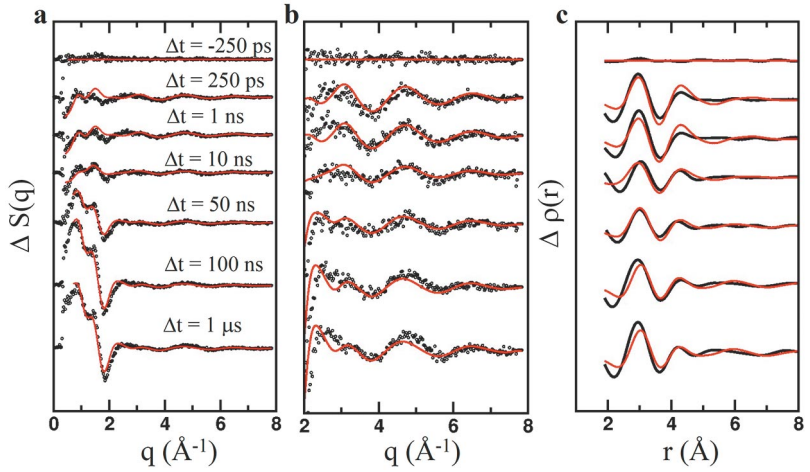

FIG. 2 (color). Measured x-ray scattering intensity changes ($\Delta S(q, \Delta t)$, circles) and those predicted from molecular dynamics simulations (red line) following the photoexcitation of CH_2I_2 in methanol. (a) Raw difference data in q space ($q = (4\pi/\lambda)\sin\theta$); (b) the same data shown for a smaller q domain and greater magnification to highlight higher-resolution oscillations present within the data; and (c) the same data (from 2.35 $Å^{-1} < q < 7.7$ $Å^{-1}$) premultiplied by $q \times \exp(-\beta^2 q^2)$ and Fourier transformed, generating a real-space representation of the changes in electron density, $\Delta\rho(r)$, as a function of the interatomic distances between atoms scaled by the scattering power of those atoms. Methanol expansion due to heating is visible as a growth in the measured x-ray scattering difference signal for 0.3 $Å^{-1} < q < 2.3$ $Å^{-1}$ for the longer time delays.

basis of a kinetic model for the transient populations of all photochemical species (Fig. 4) and established that the quantum yield for photoexcitation of CH_2I_2 was approximately 9%. Of the photoexcited molecules, 38% recombined geminately and were converted to CH_2I-I (path B, Fig. 1), whereas the remaining 62% of photodissociated iodine radicals escaped the solvent cage (path C, Fig. 1). While the nongeminate yield was higher that previously reported [20], the extra kinetic energy of the escaping iodine radicals due to our use of a shorter pump wavelength and higher energy per pulse (for which nonlinear effects may have arisen) can explain this discrepancy. The decay of the positive peak in $\Delta\rho(r)$ at 2.9 Å and complementary recovery of the negative peak at 3.7 Å [Fig. 2(c)] suggests a half-life for the CH_2I-I photoisomer of approximately 10 ns, which was refined to $\tau_{1/2} = 4.2$ ns during optimization of the kinetics model (Fig. 4) against all q-space data and all time points. This value is in good agreement (~5 ns) with that determined spectroscopically [20].

Iodine interatomic distances for both CH_2I-I and CH_2I_2 were refined by determining the optimal real-space agreement between theory and experiment [Fig. 2(c)] for data recorded at $\Delta t = 250$ ps. Specifically, the residue $\Sigma[\Delta\rho(r)_{\text{experiment}} - \Delta\rho(r)_{\text{theory}}]^2$ was minimized using

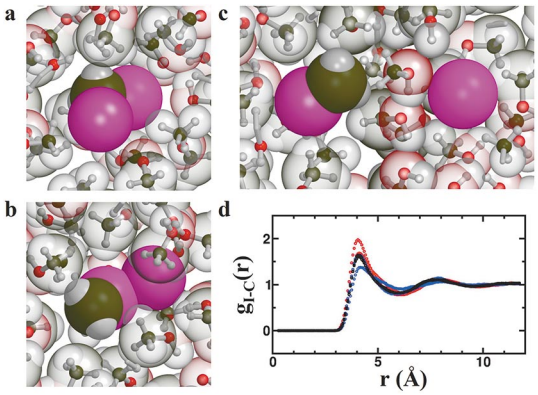

FIG. 3 (color). Solvent caging effects in methanol during the photoreaction of CH_2I_2. (a) Solvent packing around CH_2I_2; (b) Solvent packing around CH_2I-I; (c) Solvent packing around $CH_2I\cdot$ and $I\cdot$; and (d) The radial distribution function, $g_{IC}(r)$, of the interatomic distances between the iodine atoms of the solute (CH_2I_2, black; CH_2I-I, blue; $CH_2I\cdot + I\cdot$, red) and the carbon atoms of the solvent. Since x-rays are sensitive to structural changes in both the solute and the solvent, a molecular dynamics description of the entire system was used to model the experimental data (Fig. 2).

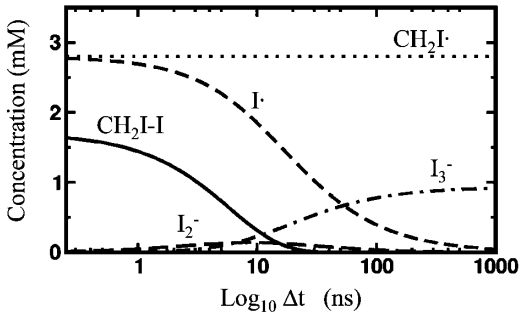

FIG. 4. Transient populations of the photochemical species following photoexcitation of CH_2I_2 in methanol. Whereas CH_2I-I relaxes directly to CH_2I_2, iodine radicals escaping the solvent cage have multiple reaction pathways: $I\cdot + e^- \rightarrow I^-$; $I\cdot + I^- \rightarrow I_2^-$; $I\cdot + I_2^- \rightarrow I_3^-$. Transient populations of CH_2I-I, $CH_2I\cdot$, $I\cdot + I^-$ (which are indistinguishable), I_2^-, and I_3^- are shown. This model was used to generate the theoretical x-ray scattering curves (red) illustrated in Fig. 2.

iterative perturbations in the iodine-iodine distance of the model, where the summations were evaluated over two domains defined by $|\Delta\rho(r)| > |\Delta\rho_{\max}(r)/2|$ about the peak at 2.9 Å, and $|\Delta\rho(r)| > |\Delta\rho_{\min}(r)/2|$ about the peak at 3.7 Å [Fig. 2(c)]. Using this protocol an iodine-iodine bond length of 3.02 ± 0.02 Å for CH_2I-I isomer and an interatomic distance of 3.50 ± 0.02 Å for the CH_2I_2 parent molecule were recovered, where the uncertainty represents the change required to double the minimum residue. These values are in good agreement with theoretical models where the predicted CH_2I-I and CH_2I_2 iodine-iodine separations were 3.03 and 3.58 Å respectively [14].

For the later time points the simplest possible reaction scheme was used to model the fate of those iodine radicals which escaped the solvent cage (Fig. 1, path C). Specifically, I· may abstract an electron from the OH group of a solvent molecule to form I^-; I· may react with I^- to form I_2^-; and I· may react with I_2^- to form I_3^- [20,33]. Each species has a structural fingerprint observable in the x-ray diffraction data. In particular, both I· and CH_2I· generate the negative feature seen in $\Delta S(q)$ for $0.3\ \text{Å}^{-1} < q < 1.2\ \text{Å}^{-1}$ for $\Delta t \leq 10$ ns [Fig. 2(a)]; I_2^- depletes features seen in $\Delta\rho(r)$ at 2.9 and 3.7 Å [Fig. 2(c)] for 10 ns $\leq \Delta t \leq$ 50 ns since its interiodine distance of 3.4 Å [33] overlaps with that of the parent molecule; and I_3^- recovers these features for $\Delta t \geq 50$ ns since it has an iodine-iodine bond length of 3.00 Å [33], similar to that of the CH_2I-I isomer. There was no signal indicating the decay of CH_2I· back to CH_2I_2, perhaps due to other species being more efficient scavengers of I· or the CH_2I· radical abstracting hydrogen ions from the solvent. Finally, the change in low-angle x-ray scattering between $0.3\ \text{Å}^{-1} < q < 2.3\ \text{Å}^{-1}$ seen for $\Delta t = 50$ ns, 100 ns, and 1 μs [Fig. 2(a)] indicates changes in the density of the solvent due to thermal expansion [32]. Thus a temperature increase of approximately 5 °C is inferred, with 50% thermal expansion occurring after 50 ns.

Because x-ray diffraction differences are explicitly sensitive to structural changes, our experimental results conclusively weigh in favor of a chemical model whereby photodissociated CH_2I_2 initially recombines by forming a covalent bond between two iodine atoms (Path B, Fig. 1) [19] rather than the dissociated iodine radical rebonding directly onto the central carbon (Path A, Fig. 1). At first sight this reaction appears analogous to the recombination reaction of I· +I· to form I_2 [5,6]. Nevertheless, it should be emphasized that the presence of a covalent bond from the iodine atom to the parent molecule's carbon atom significantly perturbs its electronic structure and we measure the interatomic I-I bond distance of the CH_2I-I isomer to be 3.02 ± 0.02 Å, significantly longer than the 2.70 Å bond distance of I_2 [33]. It testifies to the power of time-resolved x-ray diffraction that these differences in bond lengths can be accurately resolved experimentally for transient photochemical species, enabling the structural details of chemical reactions, which are otherwise inaccessible, to be probed.

We thank S. Techert for experimental help, H. Mueller for support from the ESRF Chemistry Laboratory, S. Bratos, H. Ihee, R. Vuilleumier for discussions. Data were collected at ID09B of the ESRF. This work was supported by the EU improving human potential program, the Swedish Science Research Council, and the Swedish Foundation for Strategic Research.

*Corresponding author.
†Electronic address: jand@fki.uu.se
‡Electronic address: richard.neutze@chembio.chalmers.se

[1] J. C. Williamson *et al.*, Nature (London) **386**, 159 (1997).
[2] H. Ihee *et al.*, Science **291**, 458 (2001).
[3] C. Y. Ruan *et al.*, Science **304**, 80 (2004).
[4] D. H. Paik *et al.*, Science **306**, 672 (2004).
[5] R. Neutze *et al.*, Phys. Rev. Lett. **87**, 195508 (2001).
[6] A. Plech *et al.*, Phys. Rev. Lett. **92**, 125505 (2004).
[7] N. J. Pienta and P. J. Kropp, J. Am. Chem. Soc. **100**, 655 (1978).
[8] P. J. Kropp *et al.*, Tetrahedron **37**, 3229 (1981).
[9] P. J. Kropp, Acc. Chem. Res. **17**, 131 (1984).
[10] T. Class and K. Ballschmiter, J. Atmos. Chem. **6**, 35 (1988).
[11] S. Klick and K. Abrahamsson, J. Geophys. Res. **97**, 12683 (1992).
[12] K. G. Heumann, Anal. Chim. Acta **283**, 230 (1993).
[13] R. M. Moore *et al.*, J. Geophys. Res. **C101**, 20899 (1996).
[14] M. Odelius *et al.*, J. Chem. Phys. **121**, 2208 (2004).
[15] J. Zhang and D. G. Imre, J. Chem. Phys. **89**, 309 (1988).
[16] B. J. Schwartz, J. C. King, and C. B. Harris, Chem. Phys. Lett. **203**, 503 (1993).
[17] W. M. Kwok and D. L. Phillips, Chem. Phys. Lett. **235**, 260 (1995).
[18] K.-i. Saitow *et al.*, Chem. Phys. Lett. **262**, 621 (1996).
[19] A. N. Tarnovsky *et al.*, Chem. Phys. Lett. **312**, 121 (1999).
[20] A. N. Tarnovsky *et al.*, J. Phys. Chem. A **108**, 237 (2004).
[21] Y.-L. Li *et al.*, J. Phys. Chem. A **106**, 3463 (2002).
[22] W. M. Kwok *et al.*, J. Chem. Phys. **113**, 7471 (2000).
[23] X. Zheng and D. L. Phillips, J. Phys. Chem. A **104**, 6880 (2000).
[24] M. N. Glukhovtsev and R. D. Bach, Chem. Phys. Lett. **269**, 145 (1997).
[25] A. E. Orel, Chem. Phys. Lett. **304**, 285 (1999).
[26] D. L. Phillips, W.-H. Fang, and X. Zheng, J. Am. Chem. Soc. **123**, 4197 (2001).
[27] D. L. Phillips and W.-H. Fang, J. Org. Chem. **66**, 5890 (2001).
[28] http://www.esrf.fr/computing/scientific/FIT2D/
[29] S. Bratos *et al.*, Chem. Phys. **304**, 245 (2004).
[30] D. Paschek and A. Geiger, Computer code MOSQUITO, Department of Physical Chemistry, University of Dortmund, 2002, http://ganter.chemie.uni-dortmund.de/MOSCITO
[31] B. E. Warren, *X-Ray Diffraction* (Addison-Wesley, Reading, 1969).
[32] F. Mirloup *et al.*, in *Femtochemistry and Femtobiology: Ultrafast Events in Molecular Science*, edited by H. J. T. Martin (Elsevier, New York, 2004).
[33] S. B. Sharp and G. I. Gellene, J. Phys. Chem. A **101**, 2192 (1997).